Available online at www.sciencedirect.com

jmr&t Journal of Materials Research and Technology

journal homepage: www.elsevier.com/locate/jmrt

Original Article

Estimation of physical and mechanical properties of high-strength concrete with polypropylene fibers in high-temperature condition

Heron Freitas Resende [a], *Felipe Nascimento Arroyo* [b,1], *Elvys Dias Reis* [a,1], *Eduardo Chahud* [c,1], *Herisson Ferreira dos Santos* [d,1], *José Alexandre Tostes Linhares* [e,*,1], *Afonso Rangel Garcez de Azevedo* [f,1], *André Luis Christoforo* [b,1], *Luiz Antônio Melgaço Nunes Branco* [c,1]

[a] *Dept. of Civil Engineering, Federal Center for Technological Education of Minas Gerais, Avenue Amazonas, from 4201 to 5319 - Odd Side, Belo Horizonte, Brazil*

[b] *Dept. of Civil Engineering, Federal University of São Carlos, Washington Luís Highway, km 235, São Carlos, Brazil*

[c] *Dept. of Materials and Construction Engineering, Federal University of Minas Gerais, Avenue Pres. Antônio Carlos, 6627, Belo Horizonte, Brazil*

[d] *Dept. of Civil Engineering, Federal Institute of Education Science and Technology of Rondônia, Juscelino Kubitschek Avenue - from 2717 to 2853 - Odd Side, Institutional Sector, Ariquemes, Brazil*

[e] *UENF - State University of the Northern Rio de Janeiro, LAMAV - Advanced Materials Laboratory; Av. Alberto Lamego, 2000, 28013-602, Campos dos Goytacazes, Brazil*

[f] *UENF - State University of the Northern Rio de Janeiro, LECIV - Civil Engineering Laboratory; Av. Alberto Lamego, 2000, 28013-602, Campos dos Goytacazes, Brazil*

ARTICLE INFO

Article history:
Received 26 January 2023
Accepted 8 May 2023
Available online 16 May 2023

Keywords:
Cement-based materials
Durability
High-temperature
Mechanical properties
Regression models
Synthetic fiber

ABSTRACT

High-strength concretes (HSC) have been widely applied in civil construction. However, this material does not perform well in fire situations due to spalling, a phenomenon that can be significantly mitigated by adding synthetic fibers to HSC cementitious matrix. Estimating HSC physical and mechanical properties for different compositions and temperatures can therefore be useful, as the structure may be pre-designed without requiring prior material characterization in a fire situation. With this perspective, this paper aimed to propose regression models to estimate eight properties of High-Strength Concrete with Polypropylene Fibers (HSC-PPF), namely compressive strength, tensile strength, static modulus of elasticity, dynamic modulus of elasticity, ultrasonic pulse velocity, electrical resistivity, water absorption, and weight loss, at high temperatures (up to 800 °C). For this, it was evaluated the effective correlation between mechanical responses and independent variables, such as temperature, water absorption, and dynamic modulus, and the accuracy of regression models was assessed. The results obtained indicated that, among the models proposed, the two multiple regressions were better than the simple one for estimating

* Corresponding author.
E-mail addresses: heronfr@hotmail.com (H. Freitas Resende), lipe.arroyo@gmail.com (F. Nascimento Arroyo), elvysreis@yahoo.com (E. Dias Reis), echahud@gmail.com (E. Chahud), herisson.santos@ifro.edu.br (H. Ferreira dos Santos), tosteslinhares@gmail.com (J.A. Tostes Linhares), afonso@uenf.br (A.R. Garcez de Azevedo), christoforoal@yahoo.com.br (A.L. Christoforo), luizmelg@gmail.com (L.A. Melgaço Nunes Branco).

[1] These authors contributed equally to this work.

https://doi.org/10.1016/j.jmrt.2023.05.085

HSC-PPF properties since they presented high adjustments (R^2) and low mean absolute percentage (MAPE), and coefficient of variation (CV) errors. This methodology can be used in a wide variety of fiber-reinforced HSCs.

1. Introduction

Due to the expansion of the construction industry, several studies have been done in recent years to improve the raw materials and develop concretes with better characteristics [1]. Research related to the substitution or addition of components to the concrete's cementitious matrix has been increasingly found in the literature, examples being the use of blast furnace slag [2], fly ash [3], natural fibers [4], synthetic fibers [5], and nanomaterials [6]. In this context, high-strength concrete (HSC) has gained greater applicability [7,8], mainly because of its low porosity and greater mechanical strength related to normal-strength concrete (NSC) [9]. HSC can reach 170 MPa or more of compressive strength, while NSC reaches about 40 MPa [10]. Despite the higher cost of execution, HSC has numerous advantages in terms of its application in structures, as well as potential applications in immediate risk situations, such as building fires [11].

Besides the mechanical strength, fire-resistance structural material is essential [12,13]. NSC can lose about 20% strength at 300 °C and reach 65% loss at 600 °C [14], while HSC is highly subject to explosive splintering (spalling) due to its low porosity. Thus, HSC fire resistance is lower compared to that of NSC [15]. In this sense, one of the ways to improve HSC fire resistance is by incorporating polypropylene fibers (PPFs). Huismann et al. [16] experimentally investigated the transient strain of HSC under heating up to 750 °C and the impact of PPF addition in its matrix. These authors stated that PPFs accelerate moisture transport in the range of 200–250 °C, causing drying shrinkage in the opposite direction to the free thermal stress. Uysal [17] conducted an experimental investigation to evaluate the performance of self-compacting concrete (SCC) subjected to elevated temperatures. SCC containing 30% limestone powder and no PPFs exhibited smaller reductions in strength after exposure to 200 °C compared to the same mixture containing PPFs. In addition, the authors reported severe losses in the strength of SCC with PPFs at temperatures above 600 °C but also indicated that the PPFs eliminated the risk of explosive spalling. Abdul-Rahman et al. [18], in turn, performed microstructure and structural analysis of beams produced with reactive powder concrete (RPC) with PPFs exposed to high temperature. Among several remarks, the authors pointed out that incorporating 0.25% PPFs reduced spalling and delayed beam failure by almost 2 h while using 0.75%–1.25% completely prevented both spalling and beam failure. Zeyad, Khan and Tayeh [19] partially replaced the HSC cement with volcanic pumice powder (VPP) and added PPFs. Among other findings, the authors reported that tensile strength was optimized when considering 10% VPP replacement with 0.50% PPF content and that this composition improved flexural strength but reduced HSC consistency. Given this, it is noted that the use of PPFs in cement-based materials presents numerous advantages, such as an increase in their flexural strength, and in conditions of exposure to high temperatures, a structural behavior with less damage to users [20,21].

It is worth noting the difficulty of carrying out experimental tests in a fire condition, since they can only be performed in large research centers, in addition to demanding high operating costs, whether from concrete [22], wood [23,24], or steel structures [25,26]. Thus, characterizing an HSC or even an NSC in a fire situation can be a costly and challenging task. However, if its physical and mechanical properties under different compositions and elevated temperatures are known, it is possible to create regression models to estimate them. Generally, these models are composed of independent variables that are easier to obtain experimentally, such as water absorption and others obtained from non-destructive tests (e.g., ultrasonic propagation velocity and dynamic modulus of elasticity), which are used to estimate the other HSC properties.

Two types of regression models are commonly used, the simple and the multiple ones. The first has one independent variable and the second has more than one. Furthermore, models can be linear or non-linear. Specifically, the independent variable is used to predict the dependent one in every model. Moreover, the model is also composed of parameters found using the least-squares method. To obtain a regression model with a reasonable adjustment, it is necessary to insert free variables that present a significant correlation with the variables to be estimated. In other words, variations in the independent variable effectively imply variations in the dependent one. This means that it is possible to obtain models with excellent adjustments, measured through the coefficient of determination (R^2) [27,28]. According to Montgomery [29], R^2 greater than 70% (0.70) can be considered an acceptable adjustment, and the closer to 100% (1), the better the model fit.

In the case of regression models involving cement-based materials, the independent variables can be material properties (physical or mechanical), and additive content, among others. For example, Wen, Li and Chai [30] developed multiple-variable regression models to estimate the deformation of concrete dams. Their models considered the relationship between the parameters, crest settlement, internal settlement, face slab deflection, and the dam height (H) as independent factors. In the end, it was possible to obtain models with optimal adjustments ($62.20\% < R^2 < 81.50\%$). Arroyo et al. [31] developed regression models to predict nine properties of porous plasters with micro silica (MS). These authors obtained regression models with R^2 of up to 98%, in which the MS percentage was considered an independent factor. Within nine properties estimated, seven showed R^2

greater than 70%. Lu and Wu [32], in turn, used the energy obtained in the acoustic emission test (independent factor) to estimate the tensile strength of wood. Through a multiple linear regression model, it was possible to get R^2 ranging from 83.59% to 91.83%.

With this perspective, this research aims to propose simple and multiple regression models to estimate eight properties of high-strength concrete with polypropylene fibers (HSC-PPF) at high temperatures (up to 800 °C). Specifically, in this manuscript, the HSC-PPF was characterized for compressive strength, tensile strength, static modulus of elasticity, dynamic modulus of elasticity, ultrasonic pulse velocity, electrical resistivity, water absorption, and weight loss, and the models were: (i) Simple regression, composed only of temperature; (ii) Multiple regression, composed by temperature and water absorption; (iii) Multiple regression, composed of temperature and dynamic modulus as independent variables. The dynamic modulus and water absorption were adopted as independent variables to facilitate the use of the equations since these properties are easy to obtain. The outcomes of this study are of scientific interest because, based on the adjustment's quality, it will be possible to work with several concrete mixes, additives, and other combinations, proposing more general equations to estimate HSC properties. This research is also practical since its results will allow the engineer to design the structure considering the fire action without performing previous concrete characterization.

2. Materials and methods

Ordinary Portland Cement (OPC), type CP V-ARI RS (ASTM III) manufactured by Holcim (Brazil) was used. The fine aggregate was characterized by fineness modulus and maximum characteristic diameter, 2.86 and 2.40 mm, respectively. Gneiss 1 gravel was used for the coarse aggregate, with a fineness modulus of 7.03 and a maximum diameter of 25 mm. The characterization of both aggregates followed the recommendations of ABNT NBR 7211 [33]. Two plasticizing admixtures (MIRA SET 278 and MIRA FLOW 929) were considered to improve workability and reduce water consumption. Micro silica and polypropylene fibers were added to increase the final mechanical strength [31,34,35]. The polypropylene fibers (Fig. 1) were 12 mm long monofilament type, 25 μm in diameter, and 0.91 kg/m^3 in density supplied by Viapol (Brazil).

The concrete mixing ratio was 1:1.4:1.4:0.35 (cement: sand: gravel: water) along with 2 kg/m^3 of polypropylene fibers—dosage indicated by the manufacturer, recommended by Eurocode 2 [14] and employed by the literature [36]. Table 1 presents the proposed composition.

The mixture was carried out in a 320-L concrete mixer, yielding 81 specimens measuring 10 × 20 cm^2. All inputs were mixed for about 15–18 min, as indicated in the literature [37,38] for concrete with a low water-cement ratio (w/c). The specimens were molded on a vibrating table, according to the RILEM TC 200-HTC protocols [39]. After molding (Fig. 2a), the specimens were covered with plastic to prevent water loss, according to RILEM TC 129-MTH guidelines [40]. Finally, after demolding, the specimens were stored in the moisture condition "d" (drying concrete) until completed at least two months (Fig. 2b). A room temperature of 20 ± 2 °C with a relative humidity of 50 ± 5% were considered. In the end, the samples were rectified and prepared for the tests.

Fig. 1 – Polypropylene fibers.

2.1. Treatments

As shown in Table 2, the properties were obtained at six different temperature levels. A constant rate of 1 °C/min was used for heating and cooling the specimens. The specimen was kept for 1 h at the temperature level considered in each treatment (Fig. 3a). The temperature distribution inside the oven was monitored by thermocouples installed at different points (Fig. 3b).

The following properties were evaluated for each treatment, totaling 480 specimens (10 per property): compressive strength, tensile strength, static modulus of elasticity, dynamic modulus of elasticity, ultrasonic velocity, electrical resistivity, water absorption, and weight loss.

2.2. Experimental tests

2.2.1. Compressive strength

The axial compressive strength (CS) was determined according to ABNT NBR 5739 [41]. The EMIC hydraulic testing machine (PC 200 CS model, Fig. 4) equipped with a 2000 kN load cell was used. The results were recorded using the TESC – TestScript software.

Table 1 – Concrete mixing ratio chart.

Material	Consumption (kg/m^3)
Cement	569.40
Microsilica	56.94
Sand	796.80
Gravel	796.80
MIRA FLOW 929	4.56
MIRA SET 278	4.56
Water	187.90
Polypropylene Fiber	2.00

Fig. 2 – Specimens after molding (a) and stored at room temperature (b).

Table 2 – Experimental treatments (Tr).

Tr	T (°C)
1	25
2	100
3	200
4	400
5	600
6	800

2.2.2. *Tensile strength via compression testing*

It is possible to determine the tensile strength (TS) with the diametral compression test. The tensile test was performed following ABNT NBR 7222 [42], in which cylindrical specimens were used. As shown in Fig. 4, the specimens are tested horizontally using the same machine described in the compression tests.

The equation used to determine the tensile strength through the diametral compression test is expressed below [42]. From this equation, "F" is the maximum load, "d" is the specimen diameter, and "L" is the specimen length.

$$TS = \frac{2 \cdot F}{\pi \cdot d \cdot L} \rightarrow [MPa] \quad (1)$$

2.2.3. *Static and dynamic modulus of elasticity*

The static modulus of elasticity is determined using an extensometer in the compression test (Fig. 5). The strain gauge, which has an initial length (L_0) equal to 100 mm, was fixed in the central specimen part at a distance from the base equal to two-thirds of the specimen diameter. This test follows the protocols described in the ABNT NBR 8522 [43], in which the loading takes place in cycles. The load must be applied increasingly until reaching 30% of its breaking strength, which is maintained for 60 s. Afterward, a reduction is made to 0.50 MPa with the same application speed, remaining in this condition for 60 s. This cycle is performed three times, and in its last cycle, the deformations suffered by the concrete are recorded.

The static modulus of elasticity (Es) is calculated using Eq. (2), where "σ_b" is the maximum stress, considering 30% of the compressive strength; "ε_b" is the specific strain under maximum stress, and "ε_a" the specific strain under basic stress (0.50 MPa).

$$Es = \frac{\sigma_b - 0.50}{\varepsilon_b - \varepsilon_a} \rightarrow [GPa] \quad (2)$$

whenever the natural frequency of vibration of a body coincides with the frequency of external excitation, a phenomenon called resonance occurs, which depends on the type and size of the sample. Generally speaking, the greater the distance the sound wave travels, the lower the resonant frequency. The dynamic modulus of elasticity was determined according to the Forced Resonant Frequency method, as

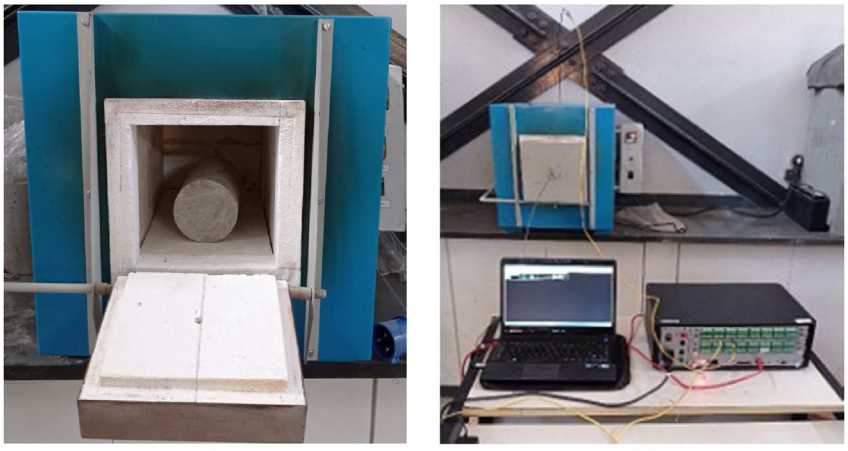

Fig. 3 – Specimens in the oven (a) and heating test using thermocouples (b).

Fig. 4 – Specimen position in tensile strength test: (a) Front view; (b) Side view.

shown in Fig. 6. The tests were performed on the Erudite MKII Resonance Frequency Test System (C.N.S. Electronics) based on the assumptions of ASTM C215-08 [44] and BS 1881: Part 209 [45]. The Resonant Frequency value can be determined using an oscilloscope described in the equipment manual [46].

Eq. (3) is used to determine the dynamic modulus of elasticity (Ed). It is worth mentioning that this formula is for cylindrical specimens [44,45,47].

$$Ed = 5.093 \cdot \frac{L}{d^2} \cdot m \cdot f_r \cdot 10^{-9} \rightarrow [GPa] \quad (3)$$

where: "f_r" is the resonant frequency, "L" is the specimen length, "γ" is the specimen specific mass, "d" is the specimen diameter and "m" is the specimen mass.

Fig. 5 – Static modulus of elasticity test with the strain gauge detail used.

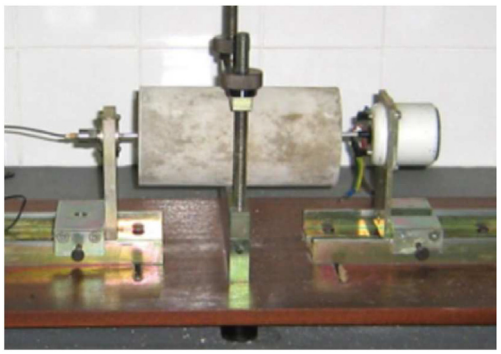

Fig. 6 – Dynamic modulus of elasticity by Resonant Frequency Method.

2.2.4. *Surface electrical resistivity*

This test was based on the four-electrode method proposed by Wenner [48]. The resistivity is measured by the potential difference between the internal electrodes, which produce an alternating electric current with up to 40 Hz. The measurement is performed by applying an electric current through the external electrodes. The internal electrodes indicate a potential difference to determine the material's electrical resistivity [49]. The Proceq surface electrical resistivity device was used [49], with a standard spacing equal to 50 mm, developed for reading specimens of 10 × 20 cm^2 or larger pieces. The data is read by the RESIPOD equipment (Proceq) [49], considering a 40 Hz frequency, as indicated by Wenner [48]. The reinforcement corrosion intensity is determined in terms of electrical resistivity, as shown in Table 3. The lower the corrosion risk, the better the concrete. Eq. (4) is used to calculate the electrical resistivity (ER), where "a" is the distance between the electrodes, "V" is the voltage measured between the central electrodes, and "I" is the electric current.

$$ER = \frac{2 \cdot \pi \cdot a \cdot V}{I} \rightarrow [\Omega m] \quad (4)$$

2.2.5. *Water absorption*

The water absorption test was carried out according to ABNT NBR 9778 [51]. Initially, the specimen is dried in an oven at 100 ± 5 °C for 72 h, and its dry mass is determined. Then, the samples are immersed in water 23 ± 2 °C for 72 h, the extra moisture is removed with a damp cloth, and the wet mass is measured. In the end, it is possible to determine the water absorption (Abs) through Eq. (5). From this equation, "m_{sat}" is the wet specimen mass (saturated with water), and "m_s" is the dry specimen mass (without water).

Table 3 – Corrosion intensity in terms of electrical resistivity.

Resistivity (Ωm)	Corrosion risk
<50	Very high
50 a 100	High
100 a 200	Low/moderate
>200	Low

Source: Adapted from Figueiredo [50].

$$Abs = 100 \cdot \frac{m_{sat} - m_s}{m_s} \rightarrow [\%] \quad (5)$$

2.2.6. Weight loss

The specimen weight loss (WL) during the test can be determined by the difference between the masses before (m_1) and 24 h after heating (m_2), using Eq. (6). The weighing scale has 0.1 kg resolution and 100 kg capacity.

$$WL = 100 \cdot \frac{m_1 - m_2}{m_2} \rightarrow [\%] \quad (6)$$

2.2.7. Ultrasonic speed

This test method is based on the propagation of high-frequency sound waves through the analyzed material. The ultrasonic speed (US) varies due to the number of voids and pores, enabling the detection of discontinuities in the concrete. A Proceq ultrasound testing equipment (RESIPOD model) was used to perform the test. Table 4 shows the concrete quality depending on the ultrasonic speed [52,53].

2.3. Statistical analysis

The Tukey means contrast test, at a 5% significance level, was used to compare the responses tested at different temperature levels (25, 100, 200, 400, 600, and 800 °C). From Tukey's test, A denotes the treatment associated with the highest mean value of a given property, B is the second highest mean value, and so on. Equal letters imply treatments with means that are statistically equivalent to each other.

After evaluating the influence of temperature levels, the correlation (Pearson correlation: $1 \leq r \leq 1$) between the properties considered in the present research was also evaluated. Analysis of Variance (ANOVA, 5% significance) was used to verify the significance of the tested correlation. By formulating this test, p-value (p probability) less than 0.05 indicates that the correlation is significant, and not significant otherwise.

After testing the correlations, linear regression models (Eq. (7)) were used to estimate the investigated properties as a function of temperature. Regression models dependent on temperature and water absorption (Eq. (8)) and temperature and dynamic modulus of elasticity (Eq. (9)) were considered to improve the model accuracy in estimating the properties. Furthermore, it allows a better understanding of the interaction between these variables. As mentioned before, the independent variables adopted were the properties that were easy to obtain experimentally (dynamic modulus and water absorption).

Table 4 – Concrete quality as a function of ultrasonic speed.

Ultrasonic speed (m/s)	Concrete quality
US > 4500	Excellent
3500 < US < 4500	Great
3000 < US < 3500	Good
2000 < US < 3000	Regular
US < 2000	Bad

Source: Adapted from BS EN 12504 [52] and Muduli and Mukharjee [53].

$$Y = \alpha_0 + \alpha_1 \cdot T + \varepsilon \quad (7)$$

$$Y = \alpha_0 + \alpha_1 \cdot T + \alpha_2 \cdot Abs + \alpha_3 \cdot T \cdot Abs + \varepsilon \quad (8)$$

$$Y = \alpha_0 + \alpha_1 \cdot T + \alpha_2 \cdot E_d + \alpha_3 \cdot T \cdot E_d + \varepsilon \quad (9)$$

From Eqs. (7)–(9), Y is the dependent variable, α_i are the parameters adjusted by the least-squares method, T is the temperature, Abs is water absorption, E_d is the dynamic modulus of elasticity, and ε is the random error. It is worth noting that Abs and E_d were considered independent variables because they are properties of easy experimental determination.

The regression model precision was evaluated by the coefficient of determination (R^2 – Eq. (10)), by the coefficient of variation (CV – Eq. (11)), and by the mean absolute percentage error (MAPE – Eq. (12)). From these equations, $Y_{data,i}$ is the sample value of a property determined experimentally, $\overline{Y}_{data,i}$ the mean value obtained from the n sample values obtained experimentally, and $Y_{predict,i}$ is the property estimated value by the regression model.

$$R^2(\%) = 100 \cdot \left(1 - \frac{\sum_{i=1}^{n} \left(Y_{predict_i} - Y_{data_i} \right)^2}{\sum_{i=1}^{n} \left(Y_{data_i} - \overline{Y}_{data_i} \right)^2} \right) \quad (10)$$

$$CV(\%) = 100 \cdot \frac{\sqrt{\sum_{i=1}^{n} \frac{\left(Y_{predict_i} - Y_{data_i} \right)^2}{n}}}{\overline{Y}_{data_i}} \quad (11)$$

$$MAPE(\%) = 100 \cdot \frac{1}{n} \cdot \sum_{i=1}^{n} \left| \frac{Y_{predict_i} - Y_{data_i}}{Y_{data_i}} \right| \quad (12)$$

The Anderson-Darling normality test (5% significance) was used to validate the Tukey test results, the ANOVA (5% significance) of the regression models and correlation tests. According to the test formulation, a p-value greater than or equal to the significance level implies a normal distribution condition.

3. Results and discussion

3.1. Concrete properties

Fig. 7 presents the mean values, the extreme values of the coefficients of variation (CV), the mean confidence intervals (CI – 95% reliability), and the results of Tukey's means contrast test (5% significance) of the six experimental treatments evaluated. It is worth mentioning that the p-values of the Anderson-Darling normality test ranged from 0.092 to 0.673, which validates (p-value $\geq$0.05) the Tukey test results.

The concrete's CS is the most used and most important parameter in structural design [54]. In HSC, CS is higher than

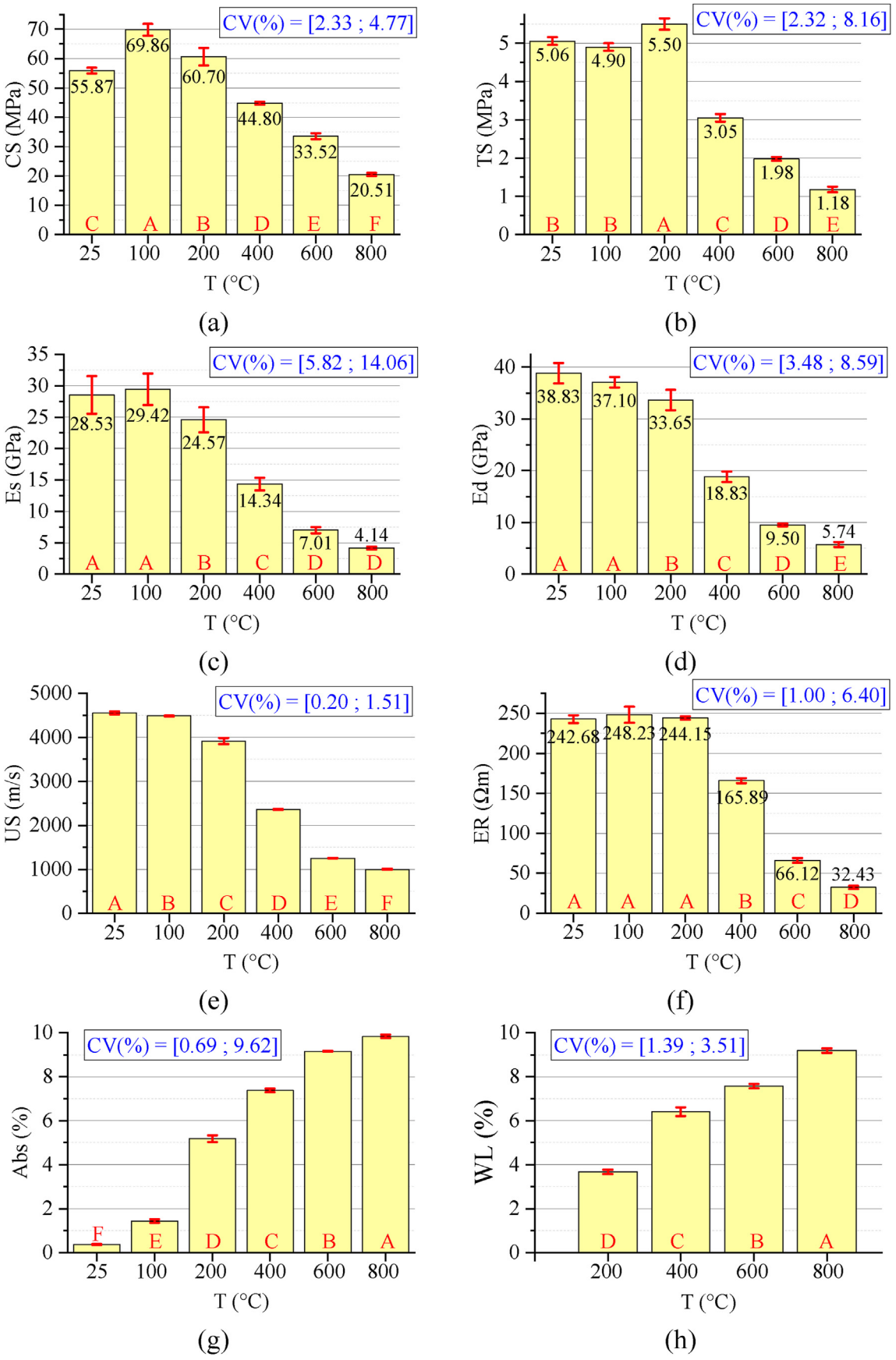

Fig. 7 – Results of the 12 treatments considered for each property: (a) CS—Compressive strength; (b) TS—Tensile strength; (c) Es—Static modulus of elasticity; (d) Ed—Dynamic modulus of elasticity; (e) US—Ultrasonic speed; (f) ER—Electrical resistivity; (g) Abs—Water absorption; (h) WL—Weight loss.

Table 5 – Pearson correlations and ANOVA (5% significance) for correlations.

Prop	Stat.	CS	TS	Es	Ed	US	ER	Abs
TS	r	0.968						
	p-value	0.000						
Es	r	0.965	0.976					
	p-value	0.000	0.000					
Ed	r	0.964	0.989	0.982				
	p-value	0.000	0.000	0.000				
US	r	0.959	0.990	0.983	0.993			
	p-value	0.000	0.000	0.000	0.000			
ER	r	0.976	0.970	0.978	0.977	0.982		
	p-value	0.000	0.000	0.000	0.000	0.000		
Abs	r	−0.972	−0.986	−0.987	−0.988	−0.992	−0.990	
	p-value	0.000	0.000	0.000	0.000	0.000	0.000	
WL	r	−0.985	−0.988	−0.972	−0.978	−0.971	−0.967	0.980
	p-value	0.000	0.000	0.000	0.000	0.000	0.000	0.000

50 MPa [55], evidencing that the concrete manufactured in the present research fits into this group. The Tukey test shows that all temperature ranges affected the CS, with 100 °C and 200 °C being the two highest strength values, respectively. At 800 °C, the HSC loses 70.64% strength compared to the maximum. Higher CS is achieved at lower temperatures (100 °C and 200 °C) since the PPFs start melting after 300 °C [56]. This increase may be due to unreacted silica fume, which reacts with cement and hydrates, producing calcium silicate hydrates C–S–H [57]; to the reinforcement of the hydrated cement paste after evaporation of free water, which increases van der Waals forces [58]; or to hydration of dehydrated cement grains and calcium oxide carbonation [59]. Besides, a slight increment in strength during fiber melting can be attributed to the porosity increase, which facilitates the escape of water vapor pressure. Some articles in the literature, however, contradict this argument by claiming loss of strength only at temperatures above 600 °C [60]. It is also worth noting that the experimental conditions affect the final results [56,61].

As well as in CS, HSC-PPF also showed improvements in TS at 200 °C and a decrease up to 800 °C. The same mechanism at PPF's melting point justifies such behavior [56]. Another reason for the increase in TS is the autoclave effect and the creation of stronger siloxane elements [62]. The resistance loss at high temperatures is given by the tetrahedral chains of the quartz molecules that elongate and reorient themselves, which leads to a significant increase in volume, causing radial cracks around the heated sample particle perimeter [63]. Other authors state that this decrease is due to the transformation of calcium hydroxide to calcium oxide in the 400–500 °C range as well as the reduction and disintegration of C–S–H in the 400–600 °C range [64].

The modulus of elasticity of concrete is one of the parameters used in structural design, which relates the applied stress to the instantaneous deformation [65]. Both Es and Ed reduced from 100 °C, and at 600 °C and 800 °C, the values did not change. This result is consistent with the literature [66,67], which indicate that the modulus of elasticity is greater at 25 °C. Therefore, it is inferred that stiffness continuously decreases by increasing temperature due to the microcracks in the cement paste caused by the thermal cycle in the heating step and the additional effect on the cooling process [68]. It is also noteworthy that this property can be affected by factors influencing its CS [69].

As stated earlier, the concrete's US measures its quality (Table 4). The temperature inversely affects the US in all temperature ranges, i.e., it regressively reduces the concrete quality. Initially, the concrete has excellent quality, reducing from 100 °C. It is evidenced that up to 200 °C, the concrete has good quality, but it reduces to bad when the temperature is higher than 600 °C. The greater the number of cracks, the lower the US in the concrete [70]. Thereby, it is understood that the HSC-PPF quality reduces due to the PPFs evaporation, creating channels that increase the internal microcracks. It is worth noting that Yang et al. [71] found results similar to those mentioned above.

The concrete's ER is a qualitative parameter of durability, characterized by the movement of ions in the pore network and is directly linked to the moisture contained in the structure [72]. It is responsible for indicating the degree of difficulty in passing an electric current through the material, i.e., it shows the risk of corrosion (Table 3). In this case, it is noted that up to 200 °C, there was no reduction in such risk. At 400 °C, the HSC still presents a low risk of corrosion, having a high and very high risk only at 600 °C and 800 °C, respectively.

The concrete's Abs, in turn, increases progressively with the increase in temperature level. A substantial increase occurs when the temperature rises from 100 °C to 200 °C, in which there was a sharp growth. The same tendency was observed at 400 °C and 600 °C. It is understood that this increase may be due to the greater penetration of water through the voids and channels created by the melted PPFs [56].

Before discussing the results, it is worth mentioning that concrete's WL is more pronounced above 100 °C and that, below this value, there was no WL in any sample. There are many potential causes for such loss after concrete exposure to high temperatures, such as spalling or surface layer chipping [15]. As shown, the WL followed the same pattern as the Abs.

The higher the temperature, the greater the WL, attributed to the same absorption mechanism. Fibers evaporate above 600 °C, and WL is accentuated [56,73].

3.2. Correlation between properties

The correlation among properties is essential for the correct application of regression models. Table 5 presents the results of Pearson's correlation coefficients ($-1 \leq r \leq 1$) and also of the ANOVA on the correlation coefficients. It is worth mentioning that the p-values of the Anderson-Darling normality test ranged from 0.181 to 0.826, which validates (p-value ≥0.05) the ANOVA results.

All correlations were significant by ANOVA (p-value <0.05) being close to 1 or −1, which shows the strong correlation between the variables confronted. Ed and Abs, which are properties of easy determination compared to the others, can be used together with temperature to estimate other properties.

Furthermore, it is noted that the mechanical properties (CS, TS, Es, and Ed) and US increase by reducing Abs and WL. The higher the mechanical properties, the better the quality of the concrete; in contrast, the worse the risk of corrosion (ER). In this case, if a lower risk of corrosion is required, a lower-strength concrete should be considered.

3.3. Simple regression models

Fig. 8 shows the results for the temperature-dependent linear regression models. All models were considered significant by ANOVA (p-value <0.05). The p-values of the Anderson-Darling normality test also support normality conditions, ranging from 0.124 to 0.879 (p-value >0.05), which validates the regression models ANOVA results.

The eight regression models have an excellent adjustment quality ($R^2 > 87.72\%$) since they are greater than 70% [29]. Thus, it is possible to estimate the properties analyzed as a function of temperature. However, to estimate the properties through these equations, the proportion of 2 kg/m^3 of PPFs must be adopted. If values different from this are chosen, these equations will not correctly predict the estimated properties as a function of temperature, water absorption, and dynamic modulus.

The smaller the error, the better the forecast presented by the proposed models. Five models reached an error smaller than 13% and can be considered optimal for estimating properties. The concrete's US and Es led to slightly higher errors, reaching 16.42% and 21.15%, respectively. An error of 62.57% is found by the Abs, leading to poor property estimation [74].

3.4. Multiple regression models

In Eqs. (13)–(18), the multiple regression models dependent on water absorption ($0.42 \leq Abs \leq 10.10\%$) and temperature ($25 \leq T \leq 800$ °C) are presented. The models dependent on temperature and dynamic modulus [$4.83 \leq Ed \leq 42.44$ GPa] are expressed in Eqs. (19)–(24). It should be noted that for the weight loss (WL) property, unlike the other properties, the temperature ranged from 200 to 800 °C. The p-values [0.126; 0.764] obtained from the Anderson-Darling normality test of the regression models were greater than 5% (0.05), which validates the ANOVA results.

$$CS = 56.06 + 0.1691 \cdot T - 2.525 \cdot Abs - 0.0186 \cdot T \cdot Abs \Rightarrow \begin{cases} R^2 = 94.81\% \\ CV = 8.04\% \\ MAPE = 7.17\% \end{cases} \quad (13)$$

$$TS = 5.398 - 0.00777 \cdot T + 0.1833 \cdot Abs - 0.000019 \cdot T \cdot Abs \Rightarrow \begin{cases} R^2 = 92.68\% \\ CV = 12.34\% \\ MAPE = 13.91\% \end{cases} \quad (14)$$

$$Es = 29.66 + 0.0217 \cdot T - 1.542 \cdot Abs - 0.00368 \cdot T \cdot Abs \Rightarrow \begin{cases} R^2 = 93.48\% \\ CV = 14.64\% \\ MAPE = 14.86\% \end{cases} \quad (15)$$

$$US = 4753 + 0.48 \cdot T - 194.1 \cdot Abs - 0.309 \cdot T \cdot Abs \Rightarrow \begin{cases} R^2 = 96.82\% \\ CV = 8.85\% \\ MAPE = 11.79\% \end{cases} \quad (16)$$

$$ER = 243.30 + 0.156 \cdot T - 0.87 \cdot Abs - 0.04361 \cdot T \cdot Abs \Rightarrow \begin{cases} R^2 = 97.15\% \\ CV = 8.93\% \\ MAPE = 10.29\% \end{cases} \quad (17)$$

$$WL = -1.283 + 0.02586 \cdot T + 0.3057 \cdot Abs - 0.001688 \cdot T \cdot Abs \Rightarrow \begin{cases} R^2 = 98.90\% \\ CV = 6.86\% \\ MAPE = 6.22\% \end{cases} \quad (18)$$

$$CS = 36.39 - 0.0339 \cdot T + 0.608 \cdot Ed + 0.001764 \cdot T \cdot Ed \Rightarrow \begin{cases} R^2 = 92.61\% \\ CV = 9.60\% \\ MAPE = 7.09\% \end{cases} \quad (19)$$

$$TS = 0.492 - 0.000726 \cdot T + 0.1143 \cdot Ed + 0.000132 \cdot T \cdot Ed \Rightarrow \begin{cases} R^2 = 96.43\% \\ CV = 8.62\% \\ MAPE = 6.72\% \end{cases} \quad (20)$$

$$Es = 4.69 - 0.00529 \cdot T + 0.644 \cdot Ed - 0.000046 \cdot T \cdot Ed \Rightarrow \begin{cases} R^2 = 95.08\% \\ CV = 12.71\% \\ MAPE = 8.56\% \end{cases} \quad (21)$$

$$US = 1109 - 0.715 \cdot T + 92.25 \cdot Ed - 0.0260 \cdot T \cdot Ed \Rightarrow \begin{cases} R^2 = 98.81\% \\ CV = 5.42\% \\ MAPE = 5.79\% \end{cases} \quad (22)$$

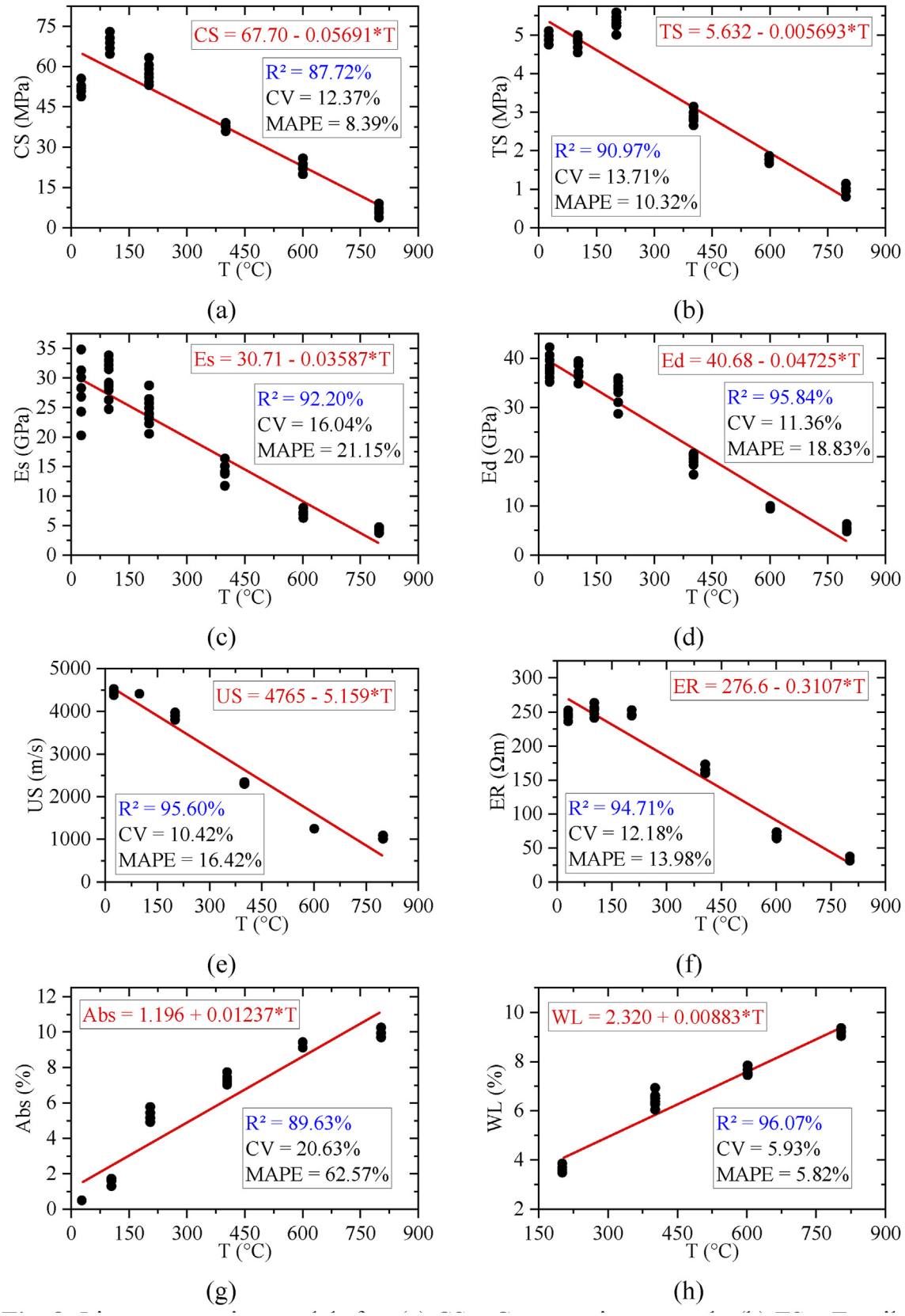

Fig. 8 – Linear regression models for: (a) CS—Compressive strength; (b) TS—Tensile strength; (c) Es—Static modulus of elasticity; (d) Ed—Dynamic modulus of elasticity; (e) US—Ultrasonic speed; (f) ER—Electrical resistivity; (g) Abs—Water absorption; (h) WL—Weight loss.

$$ER = 111.2 - 0.1758 \cdot T + 3.376 \cdot Ed + 0.007564 \cdot T \cdot Ed \Rightarrow \begin{cases} R^2 = 98.31\% \\ CV = 6.87\% \\ MAPE = 10.18\% \end{cases} \quad (23)$$

$$WL = 1.916 + 0.007574 \cdot T - 0.0554 \cdot Ed + 0.000321 \cdot T \cdot Ed \Rightarrow \begin{cases} R^2 = 98.85\% \\ CV = 3.21\% \\ MAPE = 2.54\% \end{cases} \quad (24)$$

The interactions of the following factors, temperature and water absorption (T·Abs) and temperature and dynamic modulus of elasticity (T·Ed) were considered significant by ANOVA in all investigated models, which shows that these combined factors contribute to better estimating and explaining the estimated variables. Unlike simple regression models, all multiple regression models have excellent accuracy achieved ($92.61 \leq R^2 \leq 98.80\%$; $3.21 \leq CV \leq 14.64\%$; $2.54 \leq MAPE \leq 14.86\%$) [29]. Therefore, it is evident that it is possible to estimate HSC-PPF properties by only characterizing the dynamic modulus of elasticity and water absorption responses. It is noteworthy that both tests are non-destructible and easy to perform, which brings even greater savings in the material characterization. It should be also emphasized that these results envisage new studies in which the concrete mix, and dosage of additives, among other parameters, can be used as independent factors instead of properties.

Based on the twelve (12) models analyzed, six (6) depend on the temperature and water absorption, and six (6) on the dynamic modulus of elasticity and temperature. Analyzing the same property estimated by both models, it is noticed that the multiple regression model that considers the temperature and the dynamic modulus of elasticity has minor MAPE errors for all properties. The coefficients of determination (R^2) for temperature and dynamic modulus of elasticity are more accurate in four (4) properties (TS, Es, US, and ER), while temperature and water absorption are more accurate for two (2) responses, CS and WL. Finally, analyzing the coefficient of variation, only CS had a lower CV when using temperature and water absorption as an estimator. In contrast, the other properties (TS, Es, US, ER, and WL) had lower CV when estimated by temperature and modulus of dynamic elasticity.

4. Conclusions

This research proposed regression models to estimate HSC-PPF properties (CS, TS, Es, Ed, US, ER, Abs, and WL) at high temperatures (up to 800 °C). The following conclusions can be drawn.

i. Based on the correlation of the properties, all obtained values are close to 1 or −1, i.e., the variation in any property is capable of predicting changes in the others, either increasing or reducing its value. Ed and Abs are easy to get, so they can be used together with temperature to estimate the remaining properties.
ii. Although the simple regression models presented a proper adjustment (R^2 > 70%), only 5 of 8 reached acceptable MAPE errors. Thus, using only temperature to predict the properties may not bring satisfactory results.
iii. The multiple regression models, considering either temperature and water absorption (T·Abs) or temperature and dynamic modulus of elasticity (T·Ed), provided suitable adjustments (R^2 > 70%) and low MAPE errors (MAPE <15%). These models are, in practice, quite promising since they considered easily obtainable properties via non-destructible tests.
iv. Considering the three proposed models, the two multiple regressions were better for estimating HSC-PPF properties since they presented high adjustments (R^2) and low MAPE and CV errors. Specifically, regarding these two multiple regressions, those considering temperature and dynamic modulus (T·Ed) as estimators were better than those considering temperature and water absorption (T·Abs).

These conclusions reveal that regression models similar to those proposed here can be developed in further research for other concrete types, considering various mixes, additives, and different fiber types, among other parameters. It is worth emphasizing that these manuscript findings are limited to the analysis of HSC-PPF samples with 2 kg/m^3 of PPFs and that using another dosage requires further investigation.

Financial interests

The authors declare they have no financial interests.

Declaration of competing interest

The authors declare that they have no known competing financial interests or personal relationships that could have appeared to influence the work reported in this paper.

Acknowledgements

The authors would like to thank the Brazilian Research Agency "Coordenação de Aperfeiçoamento de Pessoal de Nível Superior - Brazil (CAPES)" for the financial support provided under the Grant Code 001. The participation of A.R.G.A. was sponsored by FAPERJ through the research fellowships proc. no: E-26/210.150/2019, E-26/211.194/2021, E-26/211.293/2021, E-26/201.310/2021 and by CNPq through the research fellowship PQ2 307592/2021-9.

REFERENCES

[1] Marvila MT, Azevedo ARG, Alexandre J, Zanelato EB, Monteiro SN, Cerqueira NA. Proposal of dosing of mortars using simplex network. 2019. https://doi.org/10.1007/978-3-030-05749-7_75.
[2] Boudjehm H, Bouteldja F, Nafa Z, Bendjaiche R. Hardened properties of pre-cracked concrete incorporating metakaolin

and crushed blast furnace slag as an additional blend material. Construct Build Mater 2022;352:129009. https://doi.org/10.1016/j.conbuildmat.2022.129009.
[3] Asa E, Shrestha M, Baffoe-Twum E, Awuku B. Development of sustainable construction material from fly ash class C. J Eng Des Technol 2020;18:1615–40. https://doi.org/10.1108/JEDT-06-2019-0156.
[4] Chee SS, Jawaid M, Sultan MTH, Alothman OY, Abdullah LC. Accelerated weathering and soil burial effects on colour, biodegradability and thermal properties of bamboo/kenaf/epoxy hybrid composites. Polym Test 2019;79:106054. https://doi.org/10.1016/j.polymertesting.2019.106054.
[5] Tayeh BA, Akeed MH, Qaidi S, Bakar BHA. Influence of microsilica and polypropylene fibers on the fresh and mechanical properties of ultra-high performance geopolymer concrete (UHP-GPC). Case Stud Constr Mater 2022;17:e01367. https://doi.org/10.1016/j.cscm.2022.e01367.
[6] Reis ED, Resende HF, Ludvig P, Azevedo RC De, Spitale F, Poggiali J, et al. ESSEBonding of steel bars in concrete with the addition of carbon nanotubes: a systematic review of the literature. Buildings 2022;12:1626. https://doi.org/10.3390/.buildings12101626.
[7] Xue W, Hu X, Ren D, Hu X. Seismic behavior of precast 100 MPa grade HSC frames under reversed cyclic loading. Eng Struct 2021;243:13. https://doi.org/10.1016/j.engstruct.2021.112662.
[8] Sierens Z, Cai J, Steen C Van, Verstrynge E, Li J. Bond performance of deformed steel rebars in HSC incorporating industrially produced recycled concrete aggregate. Mater Struct 2021;54. https://doi.org/10.1617/s11527-021-01639-4.
[9] Noumowe AN, Siddique R, Debicki G. Permeability of high-performance concrete subjected to elevated temperature (600 °C). Construct Build Mater 2009;23:1855–61. https://doi.org/10.1016/j.conbuildmat.2008.09.023.
[10] Nguyen T-T, Thai H-T, Ngo T, Betar M. In: Ha-Minh C, Tang AM, Bui TQ, Vu XH, Huynh DVK, editors. Cost-effective mix design for ultra-high strength concrete up to 170 MPa. CIGOS 2021, emerging technologies and applications for green infrastructure. Lecture notes in civil engineering. Singapore: Springer; 2022. https://doi.org/10.1007/978-981-16-7160-9_5.
[11] Akeed MH, Qaidi S, Ahmed HU, Faraj RH, Mohammed AS, Emad W, et al. Ultra-high-performance fiber-reinforced concrete. Part IV: durability properties, cost assessment, applications, and challenges. Case Stud Constr Mater 2022;17. https://doi.org/10.1016/j.cscm.2022.e01271.
[12] Monteiro AV, Vieira M. Effect of elevated temperatures on the residual durability-related performance of concrete. Mater Struct 2021;54. https://doi.org/10.1617/s11527-021-01824-5.
[13] Mrak M, Winnefeld F, Lothenbach B, Dolenec S. The influence of calcium sulfate content on the hydration of belite-calcium sulfoaluminate cements with different clinker phase compositions. Mater Struct 2021;54. https://doi.org/10.1617/s11527-021-01811-w.
[14] Eurocode. European Committee for Standardization. Eurocode 2: design of concrete structures – part 1.2. general rules – structural fire design; 2004. EN 1992-1-2.
[15] Lee T, Kim G, Choe G, Hwang E, Lee J, Ryu D, et al. Spalling resistance of fiber-reinforced ultra-high-strength concrete subjected to the ISO-834 standard fire curve: effects of thermal strain and water vapor pressure. Materials 2020;13:16. https://doi.org/10.3390/ma13173792.
[16] Huismann S, Weise F, Meng B, Schneider U. Transient strain of high strength concrete at elevated temperatures and the impact of polypropylene fibers. Mater Struct 2012;45:793–801. https://doi.org/10.1617/s11527-011-9798-6.
[17] Uysal M. Self-compacting concrete incorporating filler additives: performance at high temperatures. Construct Build Mater 2012;26:701–6. https://doi.org/10.1016/j.conbuildmat.2011.06.077.
[18] Abdul-Rahman M, Al-Attar AA, Hamada HM, Tayeh B. Microstructure and structural analysis of polypropylene fibre reinforced reactive powder concrete beams exposed to elevated temperature. J Build Eng 2020;29:101167. https://doi.org/10.1016/j.jobe.2019.101167.
[19] Zeyad AM, Khan AH, Tayeh BA. Durability and strength characteristics of high-strength concrete incorporated with volcanic pumice powder and polypropylene fibers. J Mater Res Technol 2020;9:806–18. https://doi.org/10.1016/j.jmrt.2019.11.021.
[20] Azevedo AR, Marvila MT, Zanelato EB, Alexandre J, Xavier GC, Cecchin D. Development of mortar for laying and coating with pineapple fiber. Rev Bras Eng Agrícola Ambient 2020;24. https://doi.org/10.1590/1807-1929/agriambi.v24n3p187-193.
[21] de Azevedo A RG, Amin M, Hadzima-Nyarko M, Saad Agwa I, Zeyad AM, Tayeh BA, et al. Possibilities for the application of agro-industrial wastes in cementitious materials: a brief review of the Brazilian perspective. Cleaner Materials 2022;3. https://doi.org/10.1016/j.clema.2021.100040.
[22] Tayeh B, Hadzima-Nyarko M, Riad MYR, Hafez RDA. Behavior of ultra-high-performance concrete with hybrid synthetic fiber waste exposed to elevated temperatures. Buildings 2023;13:129. https://doi.org/10.3390/buildings13010129.
[23] Yeoh D, Fragiacomo M, Franceschi M de, Boon KH. State of the art on timber-concrete composite structures: literature review. J Struct Eng 2011;137:1085–95. https://doi.org/10.1061/(ASCE)ST.1943-541X.0000353.
[24] Menis A, Fragiacomo M, Clemente I. Numerical investigation of the fire resistance of protected cross-laminated timber floor panels. Struct Eng Int: Journal of the International Association for Bridge and Structural Engineering (IABSE) 2012;22:523–32. https://doi.org/10.2749/101686612X13363929517659.
[25] Zhou X, Xue X, Shi Y, Xu J. Post-fire mechanical properties of Q620 high-strength steel with different cooling methods. J Constr Steel Res 2021;180:12. https://doi.org/10.1016/j.jcsr.2021.106608.
[26] Cai Z, Yu J, Tian L, Liu F, Yu K. Fire resistance of post-earthquake steel beams insulated with a novel fire-resistive coating- FR-ECC. Eng Struct 2021;246:14. https://doi.org/10.1016/j.engstruct.2021.112887.
[27] Montgomery DC, Peck EA, Vining GG. Introduction to linear regression analysis. sixth ed. Wiley; 2021.
[28] Judd CM, McClelland GH, Ryan CS. Data analysis: a model comparison approach to regression, ANOVA, and beyond. 3th ed. Routledge; 2017.
[29] Montgomery DC. Design and analysis of experiments. eighth ed. Wiley; 2012.
[30] Wen L, Li Y, Chai J. Multiple nonlinear regression models for predicting deformation behavior of concrete-face rockfill dams. Int J GeoMech 2021;21. https://doi.org/10.1061/(asce)gm.1943-5622.0001912.
[31] Arroyo FN, Christoforo AL, Salvini VR, Pelissari PIBGB, Pandolfelli VC, Luz AP, et al. Development of plaster foam for thermal and acoustic applications. Construct Build Mater 2020;262:120800. https://doi.org/10.1016/j.conbuildmat.2020.120800.
[32] Lu D, Yu W. Predicting the tensile strength of single wool fibers using artificial neural network and multiple linear regression models based on acoustic emission. Textil Res J 2021;91:10. https://doi.org/10.1177/0040517520948200.
[33] ABNT. Associação Brasileira de Normas Técnicas. Nbr 7211: agregados para concreto - requisitos 2009.

[34] Kancharla R, Maddumala VR, Prasanna TVN, Pullagura L, Mukiri RR, Prakash MV. Flexural behavior performance of reinforced concrete slabs mixed with nano- and microsilica. J Nanomater 2021:2021. https://doi.org/10.1155/2021/1754325.
[35] Pundienė I, Pranckevičienė J. The synergistic effect of adding a blend of deflocculants and microsilica on the properties of high temperature resistant lightweight concrete with cenospheres. Construct Build Mater 2020;230:11. https://doi.org/10.1016/j.conbuildmat.2019.116961.
[36] Caetano H, Rodrigues JPC, Pimienta P. Flexural strength at high temperatures of a high strength steel and polypropylene fibre concrete. Construct Build Mater 2019;227:116721. https://doi.org/10.1016/j.conbuildmat.2019.116721.
[37] Tan-Trac N, Thai H-T, Ngo T. Optimised mix design and elastic modulus prediction of ultra-high strength concrete. Construct Build Mater 2021;302:14. https://doi.org/10.1016/j.conbuildmat.2021.124150.
[38] Campos HF, Klein NS, Marques Filho J. Proposed mix design method for sustainable high-strength concrete using particle packing optimization. J Clean Prod 2020;265:15. https://doi.org/10.1016/j.jclepro.2020.121907.
[39] IULECMSS. International union of laboratories and experts in construction materials, systems and structures. RILEM TC 200-HTC : mechanical concrete properties at high temperature - modelling and applications. 2001.
[40] RILEM. Recommendations of RILEM TC 129-MHT. Test methods for mechanical properties of concrete at high temperatures. Part 8: steady-state creep and creep recovery for service and accident conditions. Mater Struct 2000;33:6–13.
[41] ABNT. Associação Brasileira de Normas Técnicas. NBR 5739. Concreto - Ensaio de compressão de corpos-de-prova cilíndricos9; 2018.
[42] ABNT. Associação Brasileira de Normas Técnicas. NBR 7222. Concreto e argamassa – determinação da resistência à tração por compressão diametral de corpos de provas cilíndricos. 2011. p. 5.
[43] ABNT. Associação Brasileira de Normas Técnicas. NBR 8522. Concreto – Determinação dos módulos estáticos de elasticidade e de deformação à compressão. 2017. p. 20.
[44] ASTM. American. Society for testing and materials. C215-8: standard test method for fundamental transverse, longitudinal, and torsional frequencies of concrete specimens, vol. 7; 2017. https://doi.org/10.1520/C0215-02.
[45] British BS. Standard. BS 1881: testing concrete. Part 209: recommendations for the measurement of dynamic modulus of elasticity. 1990. p. 8.
[46] CNS. CNS electronics operationg: manual of erudite MK II resonant frequency test System. 1995.
[47] Almeida SM de. Análise do módulo de elasticidade estático e dinâmico do concreto de cimento Portland através de ensaios de compressão simples e frequência ressonante. Belo Horizonte: Master's Thesis – Federal University of Minas Gerais; 2012.
[48] Wenner F. A method of measuring earth resistivity, vol. 12. Bulletin of the Bureau of Standards; 1916. https://doi.org/10.6028/bulletin.282.
[49] Proceq O. Equipamento para medir resistividade superficial do Concreto de maior acurácia em todo o mundo. Proceq SA 2014;4.
[50] Figueiredo EP. Ensaios eletroquímicos para avaliação da corrosão das armaduras. I Simpósio sobre ensaios não destrutivos para Estruturas de Concreto. IBRACON; 2010. p. 42.
[51] ABNT. Associação Brasileira de Normas Técnicas. NBR 9778. Argamassa e concreto endurecidos - determinação da absorção de água. índice de vazios e massa específica 2009;8.
[52] EN. European Standards. DIN EN 12504-4: Testing concrete in structures - Part 4: determination of ultrasonic pulse velocity vol. 2021:19.
[53] Muduli R, Mukharjee BB. Effect of incorporation of metakaolin and recycled coarse aggregate on properties of concrete. J Clean Prod 2019;209:398–414. https://doi.org/10.1016/j.jclepro.2018.10.221.
[54] Al-Fakher U, Manalo A, Ferdous W, Aravinthan T, Zhuge Y, Bai Y, et al. Bending behaviour of precast concrete slab with externally flanged hollow FRP tubes. Eng Struct 2021;241:112433. https://doi.org/10.1016/J.ENGSTRUCT.2021.112433.
[55] Farmy JA, Panarese WC. High-strength concrete, vol. 53; 1994.
[56] Kalifa P, Chéné G, Gallé C. High-temperature behaviour of HPC with polypropylene fibres: from spalling to microstructure. Cement Concr Res 2001;31:1487–99. https://doi.org/10.1016/S0008-8846(01)00596-8.
[57] Hiremath PN, Yaragal SC. Effect of different curing regimes and durations on early strength development of reactive powder concrete. Construct Build Mater 2017;154. https://doi.org/10.1016/j.conbuildmat.2017.07.181.
[58] Anwar Hossain KM. High strength blended cement concrete incorporating volcanic ash: performance at high temperatures. Cem Concr Compos 2006;28. https://doi.org/10.1016/j.cemconcomp.2006.01.013.
[59] Felicetti R, Gambarova PG. Effects of high temperature on the residual compressive strength of high-strength siliceous concretes. ACI Mater J 1998;95. https://doi.org/10.14359/382.
[60] Amancio FA, Rafael MFC, Dias ARO, Cabral AE. Behavior of concrete reinforced with polypropylene fiber exposed to high temperatures. Procedia Struct Integr 2018;11:91–8. https://doi.org/10.1016/j.prostr.2018.11.013.
[61] Schneider U, Diederichs U, Ehm C. Effect of temperature on steel and concrete for PCRV's. Nucl Eng Des 1982;67:245–58. https://doi.org/10.1016/0029-5493(82)90144-3.
[62] Ma Q, Guo R, Zhao Z, Lin Z, He K. Mechanical properties of concrete at high temperature—a review. Construct Build Mater 2015;93:371–83. https://doi.org/10.1016/j.conbuildmat.2015.05.131.
[63] Nijland TG, Larbi JA. Unraveling the temperature distribution in fire-damaged concrete by means of PFM microscopy: outline of the approach and review of potentially useful reactions. Heron 2001;46:253–64.
[64] Rashad AM, Zeedan SR. A preliminary study of blended pastes of cement and quartz powder under the effect of elevated temperature. Construct Build Mater 2012;29. https://doi.org/10.1016/j.conbuildmat.2011.10.006.
[65] Krahl PA, Carrazedo R, El Debs MK. Analytical solutions for rollover instability of concrete beams on elastomeric bearing pads. Eng Struct 2018;174:154–64. https://doi.org/10.1016/J.ENGSTRUCT.2018.07.041.
[66] Cifuentes H, García F, Maeso O, Medina F. Influence of the properties of polypropylene fibres on the fracture behaviour of low-, normal- and high-strength FRC. Construct Build Mater 2013;45:130–7. https://doi.org/10.1016/j.conbuildmat.2013.03.098.
[67] Gencel O, Ozel C, Brostow W, Martínez-Barrera G. Mechanical properties of self-compacting concrete reinforced with polypropylene fibres. Mater Res Innovat 2013;15:216–25. https://doi.org/10.1179/143307511X13018917925900.
[68] Cifuentes H, Leiva C, Medina F, Fernández-Pereira C. Effects of fibres and rice husk ash on properties of heated HSC. Mag Concr Res 2012;64:457–70. https://doi.org/10.1680/macr.11.00087.
[69] Malhotra HL. Design of fire-resisting structures. 1ª ed. New York: Surrey University Press; 1982.

[70] Yüksel İ, Siddique R, Ö RÖzkan. Influence of high temperature on the properties of concretes made with industrial by-products as fine aggregate replacement. Construct Build Mater 2011;25:967–72. https://doi.org/10.1016/j.conbuildmat.2010.06.085.
[71] Yang H, Lin Y, Hsiao C, Liu J-Y. Evaluating residual compressive strength of concrete at elevated temperatures using ultrasonic pulse velocity. Fire Saf J 2009;44:121–30. https://doi.org/10.1016/j.firesaf.2008.05.003.
[72] Diniz HAA. Estudo das propriedades mecânicas e dos parâmetros de durabilidade de concretos autoadensáveis com elevados teores de adições minerais submetidos à carbonatação. Rio Grande do Norte: Master's Thesis – Federal University of Rio Grande do Norte; 2018.
[73] Xiao J, Falkner H. On residual strength of high-performance concrete with and without polypropylene fibres at elevated temperatures. Fire Saf J 2006;41:115–21. https://doi.org/10.1016/j.firesaf.2005.11.004.
[74] Yufeng W, Aiguo H, Xinhua X. A data-driven study for evaluating the compressive strength of high-strength concrete. International Journal of Machine Learning and Cybernetics 2021;12:3585–95. https://doi.org/10.1007/s13042-021-01407-4.